PERGAMON

International Journal of Plasticity 17 (2001) 1367–1391

INTERNATIONAL JOURNAL OF Plasticity

www.elsevier.com/locate/ijplas

A unified model for inelastic deformation of polycrystalline materials — application to transient behavior in cyclic loading and relaxation

H. Garmestani [a,*], M.R. Vaghar [a,1], E.W. Hart [c]

[a] *FAMU-FSU College of Engineering, Department of Mechanical Engineering, Center for Materials Research and Technology (MARTECH), Center for Nonlinear Nonequilibrium Aerosciences (CeNNAS), Room 229, 2525 Pottsdamer Road, Tallahassee, FL 32310-6046, USA*

[c] *Department of Theoretical and Applied Mechanics, Cornell University, Ithaca, NY 14850, USA*

Received in final revised form 25 July 2000

Abstract

Hart proposed a unified state variable model which is capable of predicting the nonelastic deformation for low and high temperatures over a very large strain rate range. He developed these relations from experimental evidence and a heuristic consideration of micro-mechanism of deformation in polycrystalline materials. Some of the important parameters can be uniquely determined using load relaxation tests in the fully loaded regime. The model was based on the realization that the dislocation motion is limited by the dislocation glide friction and by the resistance to strong barriers to dislocation motion represented by the hardness parameter, σ^*. A transient model based on the non-steady state condition for the frictional glide process is introduced here using a microhardness parameter as a new state variable. The microhardness parameter represents the strength or the average lifetime of the mobile dislocations relative to the frictional glide viscous drag process. The evolution of the microhardness parameter is very similar to that proposed for the hardness parameter except that the recovery plays a major role. The power law relationship for the frictional glide process is shown to be a steady state condition for the transient behavior in this model. The results show that the model can predict the transient behavior for both cyclic loading and the reloading phenomena during inelastic deformation and load relaxation.

Keywords: A. Inelasticity; A. Transient; A. Internal stress; B. State variable modeling; B. Cyclic loading

* Corresponding author. Tel.: +1-850-644-5993; fax: +1-850-644-9281.

E-mail address: garm@magnet.fsu.edu (H. Garmestani).

[1] Presently at Bennedict and Associates, Tallahassee, FL, USA.

0749-6419/00/$ - see front matter
PII: S0749-6419(00)00089-9

1. Introduction

There has been an extensive amount of research in the development of a unified phenomenological model for the inelastic deformation response of metals under various temperatures and loading conditions. The state variable approach has received a considerable attention in the mechanics community since the whole deformation history can be stored in a few state variable parameters. For a successful phenomenological model, three main conditions should be satisfied. First, it should cover important ranges of loading conditions and temperatures. Second, it should be micromechanically based. Third, it should contain the least number of state variables. It is usually possible to fit any number of complex phenomena with a series of complex functions and the task is then to calculate the constants for these complex functions. State variable approach has been under constant criticism for the fact that the parameters are used in a curve fitting scheme and no relation exists between the parameters and the microstructure. For a useful phenomenological model it is important to have the lowest number of state variables that are physically justifiable and are based on micromechanical considerations.

For the polycrystalline material, the internal state variables define the current state of deformation. This means that at any point in the deformation history the knowledge of these state variables provides complete information on the materials behavior at any later time. This is one reason that the unrecoverable plastic strain is not a state variable. Inelastic strain rate can be assumed a function of the applied stress, temperature and a set of internal state variables X_i.

$$\dot{\varepsilon} = f(\sigma, T, \ X_1, \ X_2, ...X_n) \tag{1}$$

In reality only a few of these state variables are necessary to define the mechanical behavior for a broad range of applications. This also means that the measurement of these internal state variables should not require the knowledge from the prior deformation history. It should be possible to find a special deformation path such that the change in one or more of the state variables are either constant or are fully predictable.

Most models concentrate on the steady-state region of the deformation history or the fully loaded region of the tensile test and creep. Treatment of the transient deformation associated with cyclic loading and reloading (Bauschinger effect) phenomena and load relaxation is usually treated as following a different deformation mechanism. A unified approach to incorporate these two types of deformation modes requires a fundamental understanding of the underlying micromechanics of inelastic deformation behavior. The phenomenological approach is based on a framework of continuum mechanics and the identification of the major state variable parameters responsible for the more steady-state and transient deformation. Modern understanding of dislocation theories of microscopic deformation processes has been shown to be an appropriate approach for a unified deformation model.

Constitutive relations for inelastic deformation are formulated entirely in terms of measurable flow rates, applied stress, and internal state variables that are fully

determined by macroscopic flow history. Most modern constitutive theories for inelastic deformation contain, as a state variable of the deformation behavior, an internal stress. The internal stress generally represents, also, a stored strain in the body that can to some extent be recoverable (Hart, 1976). Since the internal stress is a tensor quantity that reflects the direction of prior straining it is a source of anisotropic behavior for subsequent loading.

There are two general classes of constitutive models that describe the stress that drives the plastic flow. In the first class of models, internal stress is a direct measure of the stress driving the "plastic" flow. This class is represented in the literature only by Hart's model (Hart, 1976). In the second class of models, an effective stress that is defined as the difference between the applied stress and the internal stress drives the plastic flow. This class of models representing "kinematic hardening" is characteristic of the constitutive equations proposed by Miller (1976a,b), Robinson (1983), and Kreig et al. (1978). For a review of more recent development in these models refer to Krausz and Krausz (1996) and Simo and Hughes (1997). These models have been shown to be applicable to the more low temperature phenomena associated with cyclic loading. They have also been shown to be effective in predicting materials behavior associated with a threshold stress (overbearing stress) for high strain rate phenomena. They are, however, limited in their range of applicability to the load relaxation and creep behavior.

Attempts to introduce unified models based on the threshold stress concept resulted in the introduction of a series of internal variables and materials parameters with some physical link to the microstructure (Krausz and Krausz, 1996; Simo and Hughes 1997). The division of the stress into two components of thermal and athermal stress, however, achieved a reasonable amount of recognition in the materials community (Follansbee and Kocks, 1988). The athermal stress has played the role of a threshold stress for many models representing the tensile deformation and cyclic loading (Nemat-Nasser, 1983; Follansbee and Kocks, 1988; Nemat-Nasser et al., 1989). The basis for the existence of a state variable for the athermal stress is usually based on a set of load relaxation experiments (Ferron and Mliha-Touati, 1987; Follansbee and Kocks, 1988). More recently these models have been investigated by Tanner, McGinty and McDowell (1999) and the results show that such models are fit to the quasistatic isothermal and high strain rate data for compression. They also showed that equations-of-state with parameters determined using constant strain rate data from monotonic loading are insufficient to describe mechanical behavior. Different forms of models based on the existence of a threshold stress have been introduced in the last few years for cyclic loading (Faruque et al., 1996), superplasticity (Khraisheh et al., 1997) and for strain aging (Gilat and Wu, 1997).

Arnold and Saleeb (1994) proposed a potential-based multiaxial, unified viscoplastic model for titanium-based matrices by using specific forms for both the Gibb's and complementary dissipation potentials. Their model holds one tensorial internal state variable that is associated with dislocation substructure, with an evolutionary law that has nonlinear kinematic hardening, and both thermal- and strain-induced recovery mechanisms. Complete potential based internal state variables are then

derived for the derivation of reversible and irreversible constitutive equations (Arnold et al., 1996). They found that the inclusion of strain-induced recovery provided the needed flexibility in modeling stress–strain and creep response of metals at low homologous temperatures without adversely affecting the high temperature response (Arnold et al., 1995). Horstemeyer and McDowell (1995) examined viscoplastic constitutive models for components subjected to inhomogeneous, non-isothermal large strain conditions in a phenomenological general internal state variable framework. They employed continuum slip polycrystal viscoplasticity (mesoscale) calculations to better understand the role of different mesoscale polycrystal modeling features for predicting macroscale finite strain behavior. Wang and Richmond (1992) presented a two-state variable constitutive model for modeling the consolidation and forming processes of powder-based porous metals. This model is suitable for materials consisting of a ductile matrix with populations of isolated and interconnected voids. It contains two internal state variables representing the matrix strength and the void volume fraction.

There has been a major difference in the approach to treat work hardening. Sample et al. (1993) proposed a two-internal state variable model that predicts the constitutive response adequately over a large temperature-strain–strain rate domain. Their model assumes additive decomposition of the flow curve into steady state flow and hardening components. This enables independent determination of parameters prescribing the evolution of each state variable from a series of simple flow curves. This also suggests two mechanisms for the work hardening behavior. Khan and Liang (1999) proposed a constitutive relation for the more high strain rate regime. Hannula (1988) investigated the work hardening behavior of some FCC metals in terms of state variable model proposed by Hart and proposed a new work hardening correlation based on the separation of athermal and thermal contributions to the work hardening coefficient. Since the original Hart's model defines work hardening primarily as an athermal process for the hardness parameter, the thermal contribution suggests a different mechanism for the frictional glide process. Jackson et al. (1981) proposed a modified phenomenological state variable model based on Hart's model. They introduced a second work hardening mechanism operating within the internal stress variable as transient deformation phenomena at stresses below macroplastic yielding by incorporating the weak barriers to dislocation motion into the model (Alexopoulos et al., 1982).

The source of the transients has been the subject of research since Zener (1948). In the more steady-state deformation conditions the transients due to anelasticity can be ignored (Dewhurst and Dawson, 1984). Alden (1987) used a theory of inelastic deformation previously applied to 304 stainless steel to study a variety of materials that differ in the degree to which dislocation motion is resisted by viscous drag forces. Essmann and Mughrabi (1979) presented phenomenological models of dislocation accumulation during deformation by taking into account the annihilation of dislocations. They proposed that during dislocation glide at low temperatures, both screw and non-screw dislocations annihilate mutually with dislocations of opposite sign approaching on closely neighboring glide planes. This study suggests a diverse transient strain rate behavior determined by the magnitude of the drag forces, but a common

steady state strain rate controlled by strain hardening (Alden, 1987). The modeling effort by Jackson et al. (1981), however, suggests that the neglect of weak barriers to dislocation motion at the dislocation pile-ups is the source of these transients.

Hart's model has been shown to predict the plastic deformation for low and high temperatures over a very large strain rate range (Hart, 1976). It contains an incremental description of inelastic deformation behavior that enables a set of state variables to fully account for any previous complex loading history. He developed the form of these relations from experimental evidence and a heuristic consideration of micro-mechanism in the material (Hart, 1976, 1984). Some of the important parameters can be uniquely determined using load relaxation tests in the fully loaded regime. A simple power law relationship was defined for the frictional glide. The model showed some difficulties in predicting the more non-steady conditions due to transient deformation. In the present paper it is assumed that the interaction of the viscous process at non-steady conditions and the internal stress is the basis for transient behavior associated with cyclic loading, reloading, and the Bauschinger effect. Earlier attempts to correct these deficiencies resulted in a modification of the internal stress to include the transient effect (Jackson et al., 1981).

In the following sections a brief review of Hart's constitutive model will be given. The second invariant of a deviator tensor quantity for the isotropic case is calculated from

$$x = \frac{1}{2}\left(x_{ij}x_{ij}\right)^{1/2} \tag{2}$$

where x is the scalar invariant of tensor $\mathbf{x}$ and x_{ij} are the components of the tensor in the Cartesian coordinate system. An anisotropic fourth rank tensor K_{ijkl} can be used for the anisotropic case such $x = \frac{1}{2}\left(K_{ijkl}x_{ij}x_{kl}\right)^{1/2}$. This has been discussed earlier and for the rest of this paper only the isotropic case will be considered (Hart, 1976). A modification to the model, which incorporates the transients in stress relaxation and cyclic loading, will be introduced next. The model will be examined based on the results of a new testing method, inelastic strain rate control. The details of this test have already been provided in a separate paper by Hart and Garmestani (1993). A brief discussion of the testing method is also provided in Section 4.

2. Hart's model

Hart's constitutive equations are relations among the applied stress, the observable inelastic strain rate, a tensorial internal state variable, and a scalar state variable called the hardness parameter (or the isotropic hardening parameter) (Hart, 1976, 1984). Hart's model consists of three elements as shown in Fig. 1. The strain rate constraint in the material frame is given by

$$\dot{\varepsilon} = \dot{\alpha} + \frac{\mathrm{d}}{\mathrm{d}t}(\mathbf{a}) \tag{3}$$

where $\dot{\varepsilon}$, $\mathbf{a}$ and $\dot{\boldsymbol{\alpha}}$ are the deviator tensor quantities for the inelastic strain rate, anelastic strain (tensorial internal state variable), and the unrecoverable plastic strain rate, respectively. The stresses are related by

$$\boldsymbol{\sigma} = \boldsymbol{\sigma}^a + \boldsymbol{\sigma}^f \tag{4}$$

where $\boldsymbol{\sigma}$, $\boldsymbol{\sigma}^f$, $\boldsymbol{\sigma}^a$ are the deviator tensor quantities for the matrix stress, frictional glide stress, internal stress (anelastic stress), respectively. The tensorial relations may be written as,

$$\dot{\varepsilon} = \left(\dot{\varepsilon}/\boldsymbol{\sigma}_f\right)\boldsymbol{\sigma}^f \tag{5}$$

$$\dot{\alpha} = (\dot{\alpha}/\boldsymbol{\sigma}_a)\boldsymbol{\sigma}^a \tag{6}$$

$$\boldsymbol{\sigma}^a = (\boldsymbol{\sigma}_a/a)\mathbf{a} \tag{7}$$

where $\boldsymbol{\sigma}$, $\boldsymbol{\sigma}^f$, $\boldsymbol{\sigma}^a$, $\dot{\varepsilon}$, a and $\dot{\alpha}$ are the second invariance for the deviator tensor quantities.

The scalar invariant quantities are related by the following relations. The unrecoverable plastic strain rate, $\dot{\alpha}$, which represents the leakage of dislocations through strong barriers depends on the auxiliary "internal" stress $\boldsymbol{\sigma}_a$ and on the current value of the "hardness" $\boldsymbol{\sigma}^*$ according to Eqs. (8) and (9),

$$\ln\left[\frac{\boldsymbol{\sigma}^*}{\boldsymbol{\sigma}_\mathbf{a}}\right] = \left[\frac{\dot{\varepsilon}^*}{\dot{\alpha}}\right]^{\lambda} \tag{8}$$

$$\dot{\varepsilon}^* = f(\boldsymbol{\sigma}^*/G)^m \mathrm{e}^{-Q/RT} \tag{9}$$

where $\dot{\varepsilon}^*$ is a strain rate parameter, f is an experimental frequency constant, Q is an activation energy, R is the gas constant, G is the modulus of rigidity and m and λ are material constants. These constants are found to be $m \cong 4.5$, and $\lambda \cong 0.15$ for most materials (Table 1). Hart's model represents a class of modern constitutive relations that use internal stress ($\boldsymbol{\sigma}_a$) to drive plasticity. Plasticity is defined in terms of unrecoverable plastic strain represented here by $\dot{\alpha}$. This is represented by Eqs. (6)

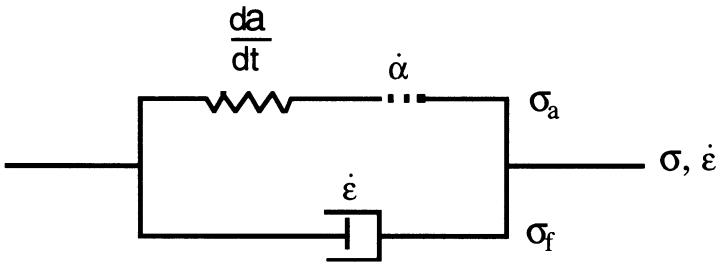

Fig. 1. Hart's constitutive model.

and (8). The inelastic strain rate, $\dot{\varepsilon}$, is a function of frictional glide stress, $\boldsymbol{\sigma}_f$, through a non-Newtonian viscous relation

$$\dot{\varepsilon} = \dot{a}^* \left[\frac{\boldsymbol{\sigma}_f}{\mu}\right]^M \tag{10}$$

where $\dot{a}^*$ is the inelastic strain rate parameter and depends only on the temperature, μ is the inelastic modulus, and M is a material constant found to be $M \cong 7.8$ for most materials. The two Eqs. (5) and (11) show that the total inelastic strain rate (which includes the anelastic strain rate) is driven by the difference between the applied stress and the internal stress. This may explain the controversy over the second class of models that may be able to predict a specific range of inelastic strain rate behavior, which includes anelasticity as a major component. This may be the case for cyclic loading and load relaxation at small strains. The anelastic strain, a, which is a state variable (through $\boldsymbol{\sigma}_a$) is related to the internal stress by Eq. (11).

$$\boldsymbol{\sigma}_a = \mu a \tag{11}$$

Work hardening and recovery of the barrier strength $\boldsymbol{\sigma}^*$ are given by,

$$\frac{\mathrm{d}\ln\boldsymbol{\sigma}^*}{\mathrm{d}t} = \Gamma(\boldsymbol{\sigma}^*, \boldsymbol{\sigma}_a)\dot{\alpha} - \mathcal{R}(\boldsymbol{\sigma}^*, T) \tag{12}$$

where $\mathcal{R}$ is the recovery term that is negligible at moderately low temperatures, and Γ is the work hardening function represented by the following equation,

$$\Gamma = C\left(\frac{\boldsymbol{\sigma}}{\boldsymbol{\sigma}^*}\right)^k \left(\frac{\boldsymbol{\sigma}^*}{G}\right)^{-m} \tag{13}$$

where C is a constant. Although there are many equations involved, only a few of them are needed for a simple application. For the rest of this work only the equations for the uniaxial tensile tests are considered.

Hart's model is shown to describe the tensile, load relaxation, and creep behavior of a number of crystalline solids under uniaxial loading when plastic flow predominates. Certain real material processes, such as large scale thermal recovery and strain-aging, are only tentatively incorporated in the recovery term, $\mathcal{R}$. It is assumed that the passage of dislocations through strong barriers results in unrecoverable plastic deformation (and the consequent hardening according to Eq. (13) and the

Table 1
Parameters of the transient model calculated from the experimental results

M	μ (MN/m^2)	λ	f (GPa)$^{-5.5}$/s	m	G (GPa)	Q/R (K^{-1})	$\dot{\varepsilon}^*$ s^{-1}	$\dot{a}^*$ s^{-1}	k
7.8	3.5×10^4	0.15	3.9E-18	4.5	3.2	25500	2.4E-6	3.5×10^{22}	8

resistance to dislocation motion produces an anelastic strain (internal stress) due to pile-up of dislocation. It was proposed that dislocation glide occurs by a viscous process and that is the basis for the apparent hysteresis and transient phenomena.

The model predicts two behaviors at low and high strain rate regions in the absence of grain boundary sliding (Fig. 2). The low strain rate regime is characterized by a concave downward behavior. This is the characteristics of the metal deformation at high homologous temperatures and is represented by Eqs. (10) and (11). The high strain rate (low temperature) region is characterized by the frictional glide processes and is represented by Eq. (12). This region exhibits a concave upward behavior as shown in Fig. 2.

3. Modified Hart's model for transient behavior

Let us define $\boldsymbol{\sigma}^t$ as a transient stress and $\boldsymbol{\sigma}^f$ as the steady-state value of the transient stress such that $\boldsymbol{\sigma}^t \rightarrow \boldsymbol{\sigma}^f$ as $\frac{\mathrm{d}\sigma_a}{\mathrm{d}t} \rightarrow 0$. The elements of the model can be related to the original Hart's model as shown in Fig. 3. The strain rate constraint in the transient element is given by

$$\dot{\boldsymbol{\varepsilon}} = \dot{\alpha}^t + \frac{\mathrm{d}}{\mathrm{d}t}\left(\mathbf{a}^t\right) \tag{14}$$

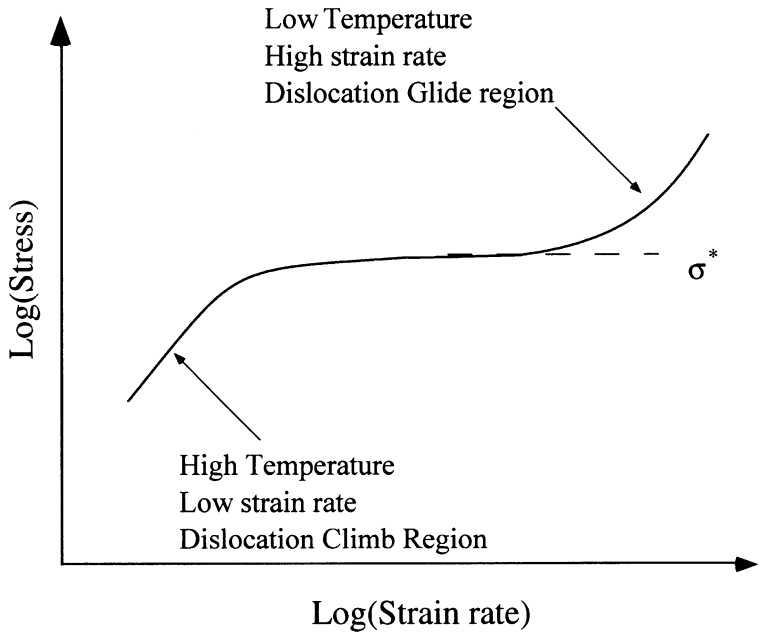

Fig. 2. Prediction of Hart's model for a very large range of temperatures and strain rates.

where $\dot{\boldsymbol{\varepsilon}}$, $\mathbf{a}^t$ and $\dot{\alpha}^t$ are the deviator tensor quantities for the inelastic strain rate, the transient strain rate (tensorial internal state variable), and the microplastic strain rate, respectively. The strain rate is also related to the plastic strain rate and the anelastic strain rate as in Eq. (3). As a matter of fact, the transient stress is linearly proportional to a transient strain through

$$\boldsymbol{\sigma}_t = \mu_t \mathbf{a}_t \tag{15}$$

where μ_t is the transient modulus. A micro-hardness parameter, $\boldsymbol{\sigma}_t^*$ is defined here which defines the strength of the viscous path. The microplastic strain is related to the transient stress through a relationship identical to the plastic strain rate relationship,

$$\ln\left(\boldsymbol{\sigma}_t^*/\boldsymbol{\sigma}_t\right) = \left(\dot{\varepsilon}_t^*/\dot{\alpha}_t\right)^{\lambda_t} \tag{16}$$

$$\dot{\varepsilon}_t^* = \dot{\varepsilon}_0\left(\boldsymbol{\sigma}_t^*/\mu_t\right)^{m_2} \tag{17}$$

where $\dot{\varepsilon}_0$, μ_τ, λ_τ, and m_2 are material constants. The evolution of the micro-hardness parameter is very similar to that of the hardness parameter except that the recovery term plays a major role,

$$\frac{\mathrm{d}\ln\boldsymbol{\sigma}_t^*}{\mathrm{d}t} = \dot{\alpha}_t\Gamma_t - \mathcal{R}_t. \tag{18}$$

We present a form for Γ_t and $\mathcal{R}_t$ (Hart and Garmestani, 1993) as

$$\Gamma_t = c_0\left[\frac{\boldsymbol{\sigma}_t}{\boldsymbol{\sigma}_t^*}\right]^{k_t}\left[\frac{\boldsymbol{\sigma}_t^*}{\mu_t}\right]^{-m_1} \tag{19}$$

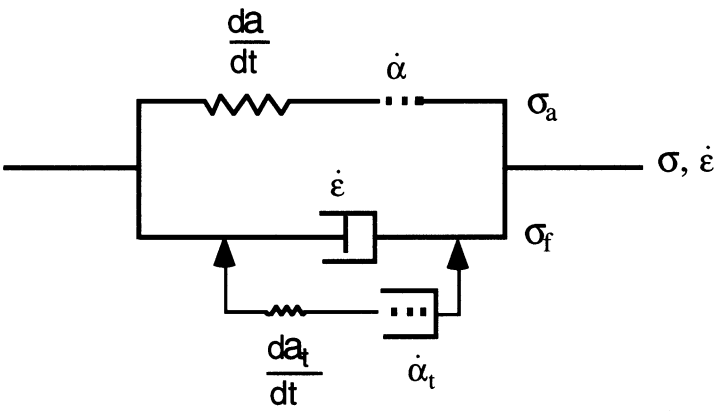

Fig. 3. The transient model in relation to Hart's model.

where

$$\mathcal{R}_t = r_0\left[\frac{\boldsymbol{\sigma}_t^*}{\mu_t}\right]^p \tag{20}$$

Both r_0 and c_0 are materials constants. Eq. (18) is very similar to Eq. (12), except that $\mathcal{R}$ in Eq. (12) is a strong function of temperature and the hardness parameter. The hardness parameter can only increase except for conditions at which recrystallization or recovery are involved. No simple form has been introduced for $\mathcal{R}$ in Eq. (12) yet, but the proposed form for $\mathcal{R}_t$ in Eq. (20) presents a strong dependence on the microhardness parameter. In Table 2 a summary of the equations listed above is presented by comparing the modified Hart's model to the original model. There are only two internal state variables for the original model model: $\boldsymbol{\sigma}^*$ and $\boldsymbol{\sigma}_a$. A new state variable, $\boldsymbol{\sigma}_t^*$ (microhardness parameter), is introduced here which represents the strength of the resistance to dislocation motion.

Table 2
The comparison of the Hart's model to modified Hart's model with the frictional glide stress as a transient element

	Hart's model	Modified Hart's model
Strain rate constraint	$\dot{\varepsilon} = \dot{\alpha} + \frac{\mathrm{d}}{\mathrm{d}t}(\mathbf{a})$	$\dot{\varepsilon} = \dot{\alpha} + \frac{\mathrm{d}}{\mathrm{d}t}(\mathbf{a})$ $\dot{\varepsilon} = \dot{\alpha}^t + \frac{\mathrm{d}}{\mathrm{d}t}(\mathbf{a}^t)$
Stress relationships	$\boldsymbol{\sigma} = \boldsymbol{\sigma}^a + \boldsymbol{\sigma}^f$	$\boldsymbol{\sigma} = \boldsymbol{\sigma}^a + \boldsymbol{\sigma}^f$ $\boldsymbol{\sigma}^f \rightarrow \boldsymbol{\sigma}^t$
Flow rules	$\dot{\varepsilon} = (\dot{\varepsilon}/\boldsymbol{\sigma}_f)\boldsymbol{\sigma}^f$ $\dot{\alpha} = (\dot{\alpha}/\boldsymbol{\sigma}_a)\boldsymbol{\sigma}^a$ $\boldsymbol{\sigma}^a = (\boldsymbol{\sigma}_a/a)\mathbf{a}$	$\dot{\varepsilon} = (\dot{\varepsilon}/\boldsymbol{\sigma}_f)\boldsymbol{\sigma}^f$ $\dot{\alpha} = (\dot{\alpha}/\boldsymbol{\sigma}_a)\boldsymbol{\sigma}^a$ $\boldsymbol{\sigma}^a = (\boldsymbol{\sigma}_a/a)\mathbf{a}$ $\dot{\alpha}^t = (\dot{\alpha}_t/\boldsymbol{\sigma}_f)\boldsymbol{\sigma}^f$ $\boldsymbol{\sigma}^t = (\boldsymbol{\sigma}_t/a_t)\mathbf{a}^t$
Scalar relationships for the internal stress	$\ln\left[\frac{\boldsymbol{\sigma}^*}{\boldsymbol{\sigma}_a}\right] = \left[\frac{\dot{\varepsilon}^*}{\dot{\alpha}}\right]^\lambda$ $\dot{\varepsilon}^* = f(\boldsymbol{\sigma}^*/G)^m \mathrm{e}^{-Q/RT}$ $\boldsymbol{\sigma}_a = \mu a$ $\frac{\mathrm{d}\ln\boldsymbol{\sigma}^*}{\mathrm{d}t} = \Gamma(\boldsymbol{\sigma}^*, \boldsymbol{\sigma}_a)\dot{\alpha} - \mathcal{R}(\boldsymbol{\sigma}^* T)$ $\Gamma = C\left(\frac{\sigma}{\boldsymbol{\sigma}^*}\right)^k \left(\frac{\boldsymbol{\sigma}^*}{G}\right)^{-m}$	The same
Scalar relationships for the frictional glide stress	$\dot{\varepsilon} = \dot{a}\left[\frac{\sigma_f}{\mu}\right]^M$	$\boldsymbol{\sigma}^t = \mu_t a_t$ $\ln\left(\boldsymbol{\sigma}_t^*/\boldsymbol{\sigma}_t\right) = \left(\dot{\varepsilon}_t^*/\dot{\alpha}_t\right)^{\lambda_t}$ $\dot{\varepsilon}_t^* = \dot{\varepsilon}_0\left(\boldsymbol{\sigma}_t^*/\mu_t\right)^{m_2}$ $\frac{\mathrm{d}\ln\boldsymbol{\sigma}_t^*}{\mathrm{d}t} = \dot{\alpha}_t\Gamma_t - \mathcal{R}_t$ $\Gamma_t = c_0\left[\frac{\sigma_t}{\boldsymbol{\sigma}_t}\right]^{k_t}\left[\frac{\boldsymbol{\sigma}_t^*}{\mu_t}\right]^{-m_1}$ $\mathcal{R}_t = r_0\left[\frac{\boldsymbol{\sigma}_t^*}{\mu_t}\right]^p$

It is clear that the modification is only performed for the frictional glide stress component of the model. As shown in Figs. 1 and 3, frictional glide stress is replaced with two other elements, which will behave as the frictional glide stress in steady-state conditions. Note that in the modified model frictional glide stress is only a limiting steady case and that is why we have replaced it with $\boldsymbol{\sigma}_t$. In reality $\boldsymbol{\sigma}_t$ and $\boldsymbol{\sigma}_f$ are the same. It is sufficient to add that such a steady-state condition corresponds to the fully loaded regions of the stress strain curve and other experimental conditions that correspond to $\mathrm{d}a/\mathrm{d}t = 0$. Such conditions can also correspond to the load relaxation once the transition occurs in the fully loaded region of the stress strain curve. The purpose of the present effort is to incorporate experimental conditions that correspond to such transients in both monotonic loading and load relaxation tests.

In the following we will show that a steady-state exists for the transient model and the modified Hart's model very simply reduces to the original Hart's model. A methodology is also presented to find a relationship among the parameters of the model and that of the original model (steady state condition).

3.1. Steady-state condition

The purpose of the present modeling effort is to incorporate the transients associated with monotonic loading and load relaxation by introducing a new state variable, micro-hardness parameter. The steady-state condition proposed here refers to non-transient conditions and should not be confused with steady-state creep conditions. A steady-state condition is defined here for the transient element such that

$$\frac{\mathrm{d}\ln\left(\boldsymbol{\sigma}_t^*/\boldsymbol{\sigma}_t\right)}{\mathrm{d}t} \cong 0, \quad \text{at} \quad \boldsymbol{\sigma}_t^* = \boldsymbol{\sigma}_{ts}^*. \tag{21}$$

During the fully loaded region this steady-state may be relaxed to the condition $\mathrm{d}\ln\boldsymbol{\sigma}_t^*/\mathrm{d}t \cong 0$. The microplastic strain rate can then have a steady-state limit such that

$$\dot{\alpha}_t = \dot{a}_t^* \left(\frac{\boldsymbol{\sigma}_t}{\mu_t}\right)^{m_t}. \tag{22}$$

A parameter v_s is defined to represent the transient strain rate sensitivity as

$$v_s = \frac{\partial \ln \boldsymbol{\sigma}_t}{\partial \ln \dot{\alpha}_t}\Big|_{\boldsymbol{\sigma}_t^* = \text{constant}}. \tag{23}$$

Substituting Eq. (22) into Eq. (23) yields $v_s = \frac{1}{m_t}$ and from Eq. (22) we may write,

$$v_s = \lambda_t \ln\left[\frac{\boldsymbol{\sigma}_{ts}^*}{\boldsymbol{\sigma}_t}\right] \tag{24}$$

or

$$\frac{\boldsymbol{\sigma}^*_{ts}}{\boldsymbol{\sigma}_t} = \exp(v_s/\lambda_t). \tag{25}$$

The microplastic strain rate at steady-state can be calculated using Eqs. (16) and (17) as,

$$\dot{\alpha}_{ts} = \dot{\varepsilon}_0 \left[\frac{\boldsymbol{\sigma}^*_{ts}}{\boldsymbol{\sigma}_t}\right]^{m_2} \left[\ln\left(\boldsymbol{\sigma}^*_{ts}/\boldsymbol{\sigma}_t\right)\right]^{-1/\lambda_t} (\boldsymbol{\sigma}_t/\mu_t)^{m_2}. \tag{26}$$

A comparison of Eqs. (22) and (26) requires that $m_2 = m_t$, and

$$\dot{a}^*_t = \dot{\varepsilon}_0 \left[\frac{\boldsymbol{\sigma}^*_{ts}}{\boldsymbol{\sigma}_t}\right]^{m_2} \left[\ln\left(\boldsymbol{\sigma}^*_{ts}/\boldsymbol{\sigma}_t\right)\right]^{-1/\lambda_t}. \tag{27}$$

Eq. (26) relates the parameters of the frictional glide stress as the steady-state limit of the transient model. A comparison of this equation and the power law relation for the frictional glide stress relationship, Eq. (10) shows that,

$$m_2 = m_t = M \tag{28}$$

and

$$\dot{a}^*_t = \dot{\varepsilon}_0 \left[\frac{\boldsymbol{\sigma}^*_{ts}}{\boldsymbol{\sigma}_t}\right]^{m_2} \left[\ln\left(\boldsymbol{\sigma}^*_{ts}/\boldsymbol{\sigma}_t\right)\right]^{-1/\lambda_t}. \tag{29}$$

If this steady-state condition is found experimentally, then $\dot{\varepsilon}_0$ can be measured from the relation

$$\dot{\varepsilon}_0 = \dot{a}^*_t \left[\frac{\boldsymbol{\sigma}^*_{ts}}{\boldsymbol{\sigma}_t}\right]^{-m_t} \left[\ln\left(\boldsymbol{\sigma}^*_{ts}/\boldsymbol{\sigma}_t\right)\right]^{1/\lambda_t}. \tag{30}$$

At steady-state, the governing equation for the evolution of the transient micro hardness parameter $\boldsymbol{\sigma}^*_t$, Eq. (18) becomes,

$$0 = c_0 \left[\frac{\boldsymbol{\sigma}_t}{\boldsymbol{\sigma}^*_{ts}}\right]^{k_t} \left[\frac{\boldsymbol{\sigma}^*_t}{\mu_t}\right]^{-m_1} \dot{\alpha}_{ts} - r_0 \left[\frac{\boldsymbol{\sigma}^*_t}{\mu_t}\right]^{p}. \tag{31}$$

Rewriting this equation to find $\dot{\alpha}_{ts}$, we get

$$\dot{\alpha}_{ts} = (r_0/c_0) \left[\frac{\boldsymbol{\sigma}^*_{ts}}{\boldsymbol{\sigma}_t}\right]^{k_t+m_1+p} \left[\frac{\boldsymbol{\sigma}_t}{\mu_t}\right]^{m_1+p}. \tag{32}$$

Equating Eqs. (32) and (26) results in,

$$\left[\frac{\boldsymbol{\sigma}^*_{ts}}{\boldsymbol{\sigma}_t}\right]^{m_2-k_t-m_1-p}\left[\ln(\boldsymbol{\sigma}^*_{ts}/\boldsymbol{\sigma})_t\right]^{-1/\lambda_t}=\frac{r_0}{c_0\dot{\varepsilon}_0}\left[\frac{\boldsymbol{\sigma}_t}{\mu_t}\right]^{m_1+p-m_2}. \tag{33}$$

If v_s is to remain constant (independent of $\boldsymbol{\sigma}_t$), then we must have,

$$p+m_1-m_2=0 \tag{34}$$

which results in,

$$\frac{r_0}{c_0}=\dot{\varepsilon}_0\left[\frac{\boldsymbol{\sigma}^*_{ts}}{\boldsymbol{\sigma}_t}\right]^{m_2-k_t-m_1-p}\left[\ln\left(\boldsymbol{\sigma}^*_{ts}/\boldsymbol{\sigma}_t\right)\right]^{-1/\lambda_t} \tag{35}$$

and $\boldsymbol{\sigma}^*_{ts}/\boldsymbol{\sigma}_t$ is independent of $\boldsymbol{\sigma}_t$. In addition, Eq. (35) determines the ratio r_0/c_0. Also from Eqs. (34) and (28) we may write,

$$m_1=m_t-p. \tag{36}$$

The steady-state condition may be achieved either at the fully loaded region of a tensile test, or in the case of a constant inelastic strain rate test (Hart and Garmestani, 1993). It can be assumed that in such a test the transition to steady-state is instant. In the following, the result of number of experiments based on the inelastic strain rate control is explained and then the model parameters are determined for the transient model.

4. Inelastic strain rate control experiments

The experimental configuration employs a strain gauge or strain transducer mounted directly on the tensile specimen. The inelastic strain ε is given to a high accuracy by the relation,

$$\varepsilon=\varepsilon_t-e \tag{37}$$

where e is the specimen elastic strain and ε_t is the total true strain. Furthermore the elastic strain may be expressed in terms of the measured applied load P by

$$e=CP \tag{38}$$

The constant C is the machine compliance and depends also on specimen geometry (Hart and Garmestani, 1993). This constant can be selected so that the elastic strain is compared directly with ε_t, and so

$$\varepsilon=\varepsilon_t-CP. \tag{39}$$

An Instron Model 1321 tension–torsion servohydraulic testing machine with analog circuitry was used for the experiments in this work which provides a command signal $\varepsilon_c(t)$ that can be compared electronically with the current value of the inelastic strain ε. The difference between ε and ε_c provides an error signal that drives the actuator. The actuator drives the load train so that the error signal is held as close to zero as possible. The imposed strain rate $\dot{\varepsilon}_c$ is controlled by an analog function generator that is in turn controlled by a digital computer and an analog-digital interface. The method of controlling constant inelastic strain rate requires that a signal proportional to the load cell feedback be subtracted from the strain input signal in real time and that the resultant difference be used as the active feedback signal. This constitutes a system with an additional closed loop circuit.

Two different kinds of experiments have been performed and discussed in this paper. They are cyclic loading at constant inelastic strain rate and abrupt changes of $\dot{\varepsilon}$ from an initial value $\dot{\varepsilon}_i$ to zero. The second experiment is a new kind of load relaxation performed under constant inelastic strain. The material chosen for the purpose of this paper is Al-1100. Both strain gages and extensometers (4% range) have been used to measure the current value of the strain on the sample. For the tests in load relaxation and cyclic loading a strain gage was used whereas for large strain amplitudes an extensometer was used.

4.1. Inelastic strain rate cyclic loading

The inelastic strain rate control circuitry has been used to produce a hysteresis loop for a high purity aluminum sample as shown in Fig. 4. The different loops are obtained using the incremental step test. One specimen is subjected to a series of blocks of gradually increasing and decreasing strain amplitude. After a few cycles the material stabilizes. At inelastic strain cycle amplitudes of 100–1300 $\mu\varepsilon$ and strain rates of 5×10^{-5} (s^{-1}) very stable cyclic loops were obtained for aluminum.

4.2. Inelastic strain rate load relaxation

Abrupt strain rate change tests are used commonly to measure the strain rate sensitivity and transient behavior of materials (Alden, 1977). The experiment involves an abrupt change in the controlled inelastic strain. The stress data is then plotted in time as the output of the experiment. Direct measurement of total strain and stress and a plot of the calculated inelastic strain will ensure the accuracy of the test. The load relaxation test is conventionally performed by loading a specimen in tension or compression to some predetermined load and extension, and subsequently recording the load as a function of time at fixed cross head position. The best testing requires a rather stiff machine (to minimize the time of the experiment), and good temperature stability and control (Lee and Hart, 1971; Hart and Solomon, 1973; Hart and Garmestani, 1993). The relaxation time is inversely proportional to the stiffness of the machine plus the specimen. A constant inelastic strain load relaxation test depends only on the inelastic property of the material under deformation.

Fig. 5 shows a load relaxation experiment from an initial inelastic strain rate of 10^{-5} (s^{-1}). The result of the loading history is plotted on a log–log scale. The load relaxation was initiated from the fully loaded region of the tensile test.

4.3. Hart's model for controlled inelastic strain rate.

Hart's model, while providing a unified description of plasticity dominated deformation, exhibits deficiencies when applied to transient deformation phenomena at stresses below macroscopic yield. In the following the results of the classical model are compared to the controlled inelastic strain rate experiments. Applying the model for this mode of deformation is very easy since the frictional glide stress and the internal stress can be analyzed independently. Frictional glide stress depends only on the inelastic strain rate through Eq. (10). As a result, frictional glide stress has a step function behavior. It is zero at zero strain rate. It abruptly changes to a value determined by Eq. (40),

$$\sigma_f = \mu(\dot{\varepsilon}/\dot{a}^*)^{-1/M} \tag{40}$$

and then remains constant until there is a change in the applied inelastic strain rate. Internal stress, however, behaves quite differently (as shown in Fig. 6). For the independent σ_a branch, the unrecoverable plastic strain may be written as,

$$\dot{\alpha} = \dot{\varepsilon}[\ln(\sigma^*/\sigma_a)]^{-1/\lambda} \tag{41}$$

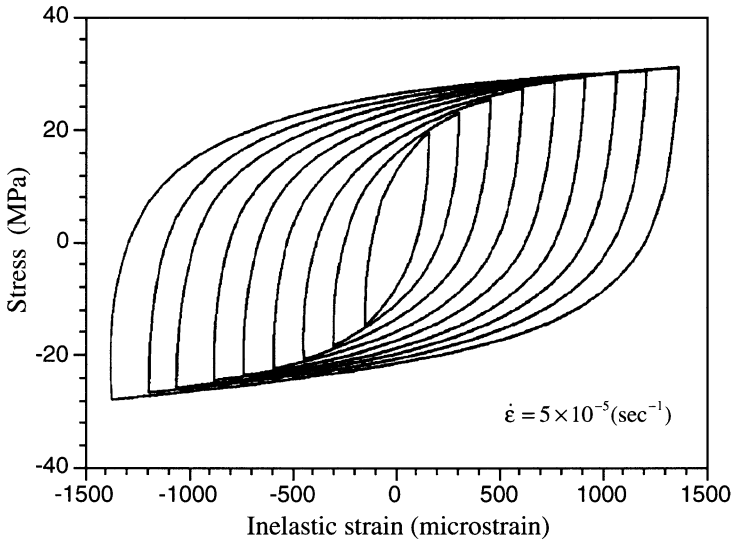

Fig. 4. Record of stress versus inelastic strain for subsequent curves of increasing inelastic strain amplitude.

Using Eqs. (3), (11) and (41) the following differential equation is derived

$$\frac{d\sigma_a}{dt} + \mu\dot{\varepsilon}[\ln(\sigma^*/\sigma_a)]^{-1/\lambda} = \mu\dot{\varepsilon} \tag{42}$$

where $\dot{\varepsilon}$ is constant. This equation is the governing equation determining the behavior of the internal stress during an experiment where the inelastic strain rate is kept constant.

Fig. 7 shows the result of the constant inelastic strain load relaxation experiment for 1100 aluminum. By performing a non-linear fit to the data σ^* and $\mu\dot{\varepsilon}^*$ are determined with a high accuracy. Independent evaluation of μ is possible at this point by finding the slope of the stress versus inelastic strain curve at the initial loading during an inelastic strain rate controlled test. More accurate measurement of μ is not necessary at this point because our intention is to show the most general behavior. The result of the simulation plotted in the same figure demonstrates the agreement between the result and the experiment.

The result of the simulation for the loading curve for an inelastic strain rate tensile test is shown in Fig. 8. The experiment data for aluminum is shown in the same plot. The model predicts a very sharp transition to the steady state value of σ_{as}. The experimental data however shows a very smooth transition. After the transition the material is fully represented by the plastic element.

Consider the region $\sigma_a < \sigma_{as}$, where plasticity is negligible. In this region the model behavior is dictated by anelastic strain. In a constant inelastic strain rate loading unloading, the model predicts a linear behavior followed by a jump represented by frictional glide stress. The return is also linear (Fig. 8). By contrast, real materials deviate from this behavior, both during loading at some fraction of the applied stress and during unloading as the stress approaches zero.

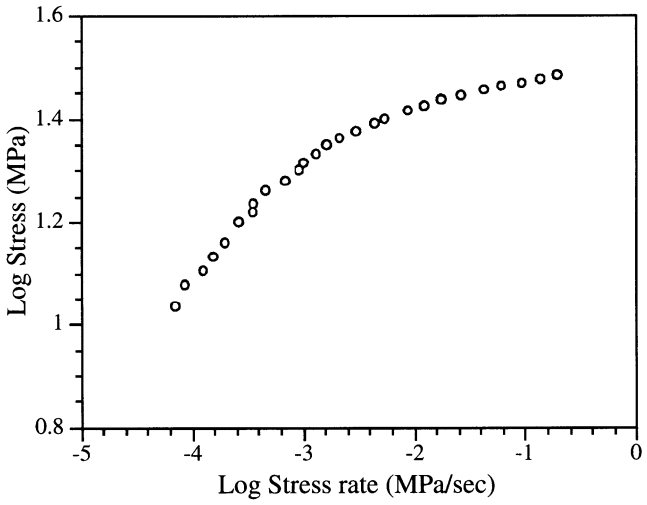

Fig. 5. Plot of log σ versus log $\dot{\sigma}$ for constant inelastic strain relaxation experiment.

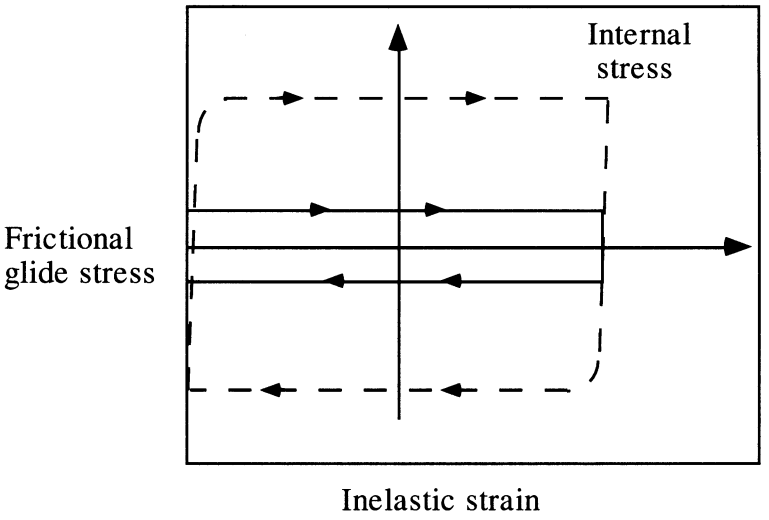

Fig. 6. Schematic diagram showing the behavior of the frictional glide stress and the internal stress for a constant inelastic strain rate test.

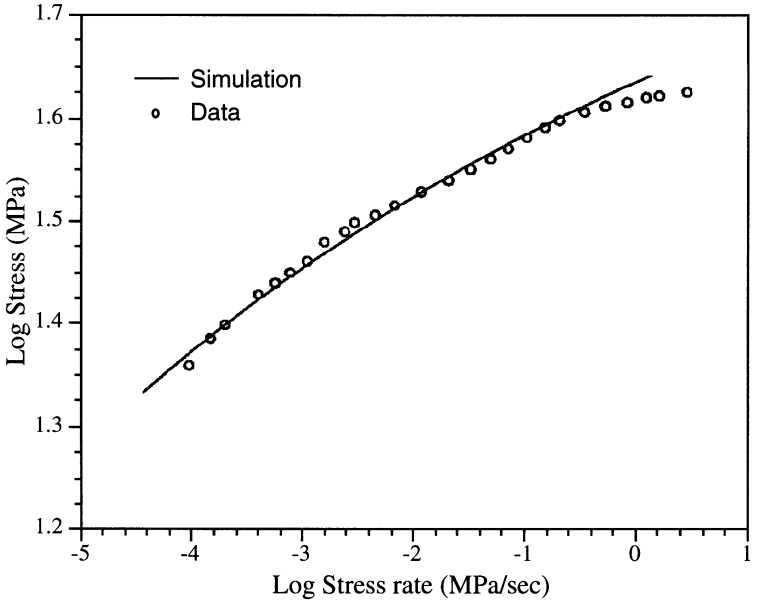

Fig. 7. Plot of log σ versus log $\dot{\sigma}$ for the simulation performed on Hart's model on the load relaxation experiment at constant inelastic strain.

From these observations, it seems that a second strain may be accumulating during deformation other than the two mentioned above. It may be concluded that the anelastic strain has a non-linear behavior. This, however, would lead us to the conclusion that after a drop to zero load all or most of this strain should recover. Such tests have been performed in this study. The result shows that even after a month of relaxation the strain recovered is only a fraction of the elastic strain. This suggests a value of anelastic modulus several times higher than elastic modulus. The transients, however, are as large as 10–20 times elastic strain, which suggests a very small value for the anelastic strain. This contradiction suggests that if the anelastic strain measured during load drop tests are truly due to anelasticity there has to be a separate phenomena explaining the transient behavior. This problem was already recognized by Hart and Solomon (1973). In the following a new model for the transient behavior will be presented such that the conventional power law for the frictional glide stress can be defined as the steady state condition.

5. Simulation and results

In a constant inelastic strain rate test cycle shown in Fig. 4, it can be assumed that a true steady state condition exists. The power law relationship in the form of Eq. (22) can then be used as shown in Fig. 9 to simulate the loading history. It was found that the power m_2 remained constant during loading. This power was found to be $m_2 = 0.17$–0.3 for aluminum.

Both μ_t and μ can be calculated from the inelastic strain rate cyclic load test. The methodology is very similar to what is described already in a model presented by Jackson et al. (1981). To find the parameters $\dot{\varepsilon}_0$ and c_0 the limiting behavior of the

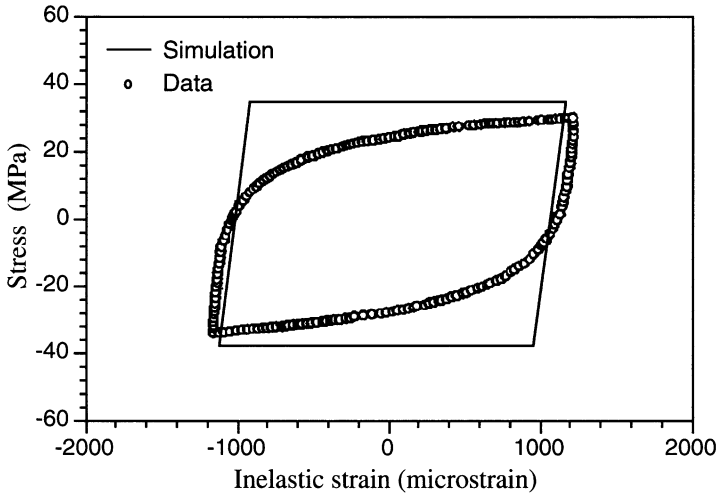

Fig. 8. Plot of stress versus inelastic strain for the experimental data and simulation results for Hart's model in the absence of work hardening.

model is considered. During loading the strain rate of the transient element cannot exceed the total imposed inelastic strain rate. This restriction provides a method to approximate some of the parameters experimentally. During full loading the steady state assumption is valid, and $\boldsymbol{\sigma}_t$ reaches to a maximum once $\dot{\alpha}_t = \dot{\varepsilon}$. If this maximum value is called $\boldsymbol{\sigma}_{tm}$ then $\dot{\varepsilon}$ can be determined from Eq. (26), and thus,

$$\dot{\varepsilon}_0 = \dot{\varepsilon}[\exp(-1/\lambda_t)](m_t\lambda_t)^{-1/\lambda_t}(\boldsymbol{\sigma}_{tm}/\mu_t)^{-m_t}. \tag{43}$$

The only variable to be determined experimentally is then $\boldsymbol{\sigma}_{tm}$. At full loading $\boldsymbol{\sigma}_t^*$ also reaches a maximum once $\dot{\alpha}_t = \dot{\varepsilon}$. Thus, Eq. (32) predicts c_0 to be

$$c_0 = (r_0/\dot{\varepsilon})\exp\left(\frac{k_t}{m_t\lambda_t}\right)\left[\frac{\sigma_{tm}^*}{\mu_t}\right]^{m_t} \tag{44}$$

where $\boldsymbol{\sigma}_{tm}^*$ is the maximum value for $\boldsymbol{\sigma}_t^*$ at steady-state. The recovery of the transient hardness parameter $\boldsymbol{\sigma}_t^*$ becomes important at low stress and during the load reversals. The data for the load reversals during a constant inelastic strain rate test can be used to determine the recovery constant r_0. The parameters used for the simulation of the numerical results are found by best fit to the experimental results as given in Table 3.

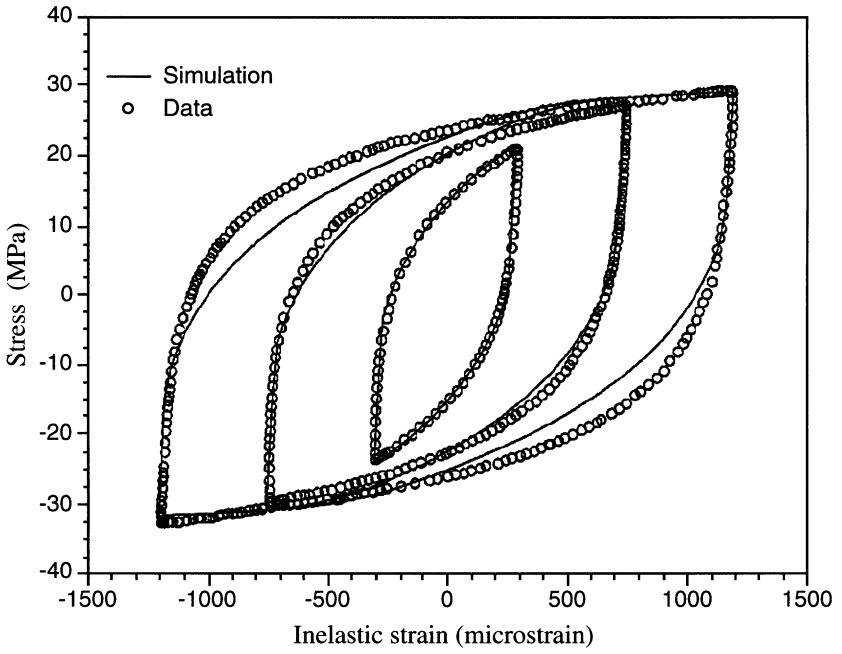

Fig. 9. Plot of stress versus inelastic strain for the experimental data and simulation results for the first class of models.

5.1. Numerical simulation for cyclic loading

A simulation of the small strain results for high purity aluminum with the transient recovery model is shown in Fig. 10. Note that no steady-state condition is assumed here and the fit is perfect. The result of the simulation shows good agreement between the result and the simulation for subsequent loading curves. The fit to the small and large strain cyclic data is also very good. This is perhaps, not too surprising, considering the additional parameters. The model can predict any curves for larger inelastic strain amplitude.

The hardness parameter $\boldsymbol{\sigma}_t^*$ recovers during unloading and at low stress levels and hardens during loading (Fig. 11). This behavior results in a smoother reloading behavior.

5.2. Numerical simulation for load relaxation data

During transient loading the unrecoverable plastic strain rate $\dot{\alpha}$ is negligible for initial loading history. Using the governing equations and since $\dot{\varepsilon}$ is zero, we get

$$\frac{\mathrm{d}\boldsymbol{\sigma}}{\mathrm{d}t} = -\dot{\varepsilon}_0 \mu_t \left(\frac{\boldsymbol{\sigma}_t^*}{\mu_t}\right)^{m_t} \left[\frac{\boldsymbol{\sigma}_t^*}{\boldsymbol{\sigma} - \mu\varepsilon}\right]^{-1/\lambda_t}. \tag{45}$$

Table 3
Parameters of the transient model calculated from the experimental results

μ (GPa)	μ_t (GPa)	λ_t	p	m_t	k_t	r_0 (s^{-1})	c_0	$\dot{\varepsilon}_0$ (s^{-1})
10.4	29.7	0.15	0.2–0.35	5.0	6-8	26.7	4.2×10^{-11}	1.2×10^{20}

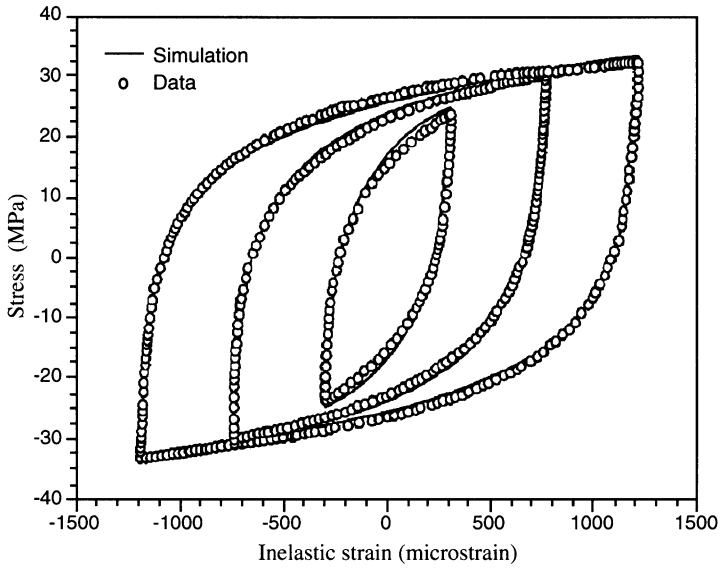

Fig. 10. Plot of stress versus inelastic strain for the experimental data and simulation results.

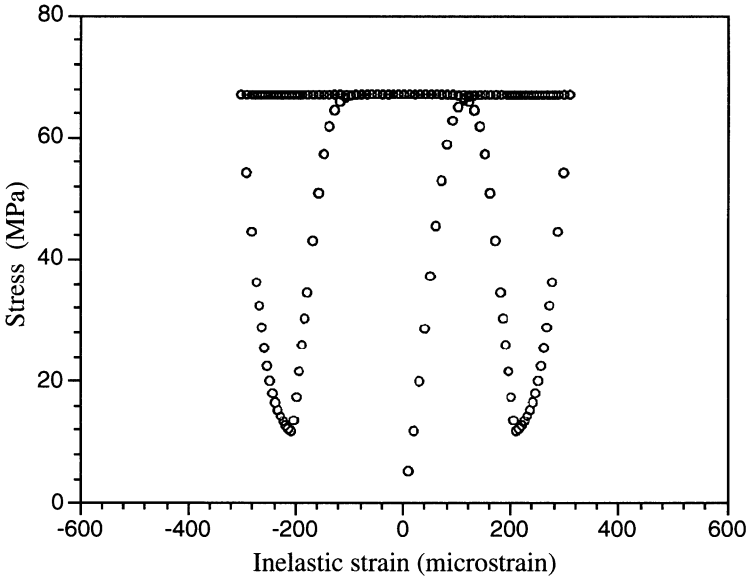

Fig. 11. Plot of σ_t^* versus inelastic strain for a constant inelastic strain rate tension–compression cycle. The results are provided only for the tensile part.

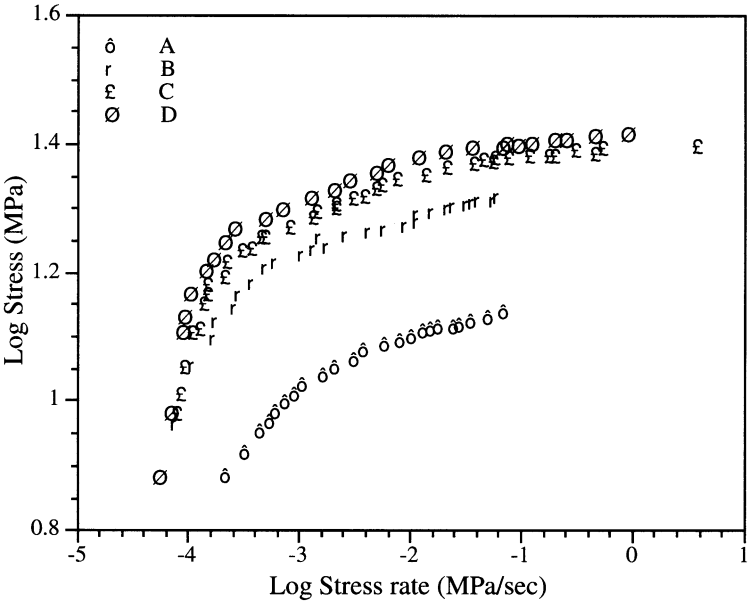

Fig. 12. Plot of log σ versus log $\dot{\sigma}$ for constant inelastic strain relaxation experiment. Each curve corresponds to the interrupt points in Fig. 13.

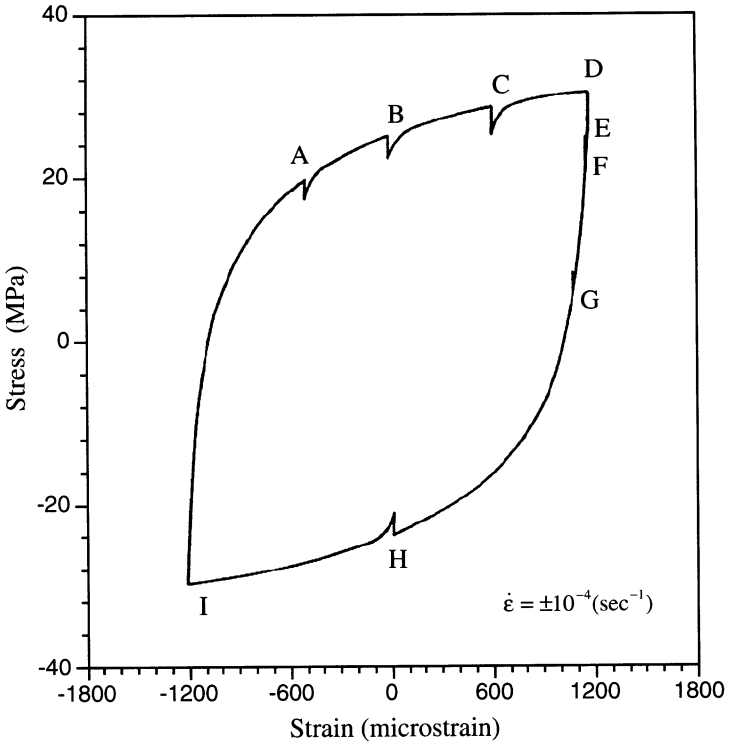

Fig. 13. Record of stress versus inelastic strain for constant inelastic strain rate test. The test was interrupted and relaxation tests were performed at interrupt points A–I.

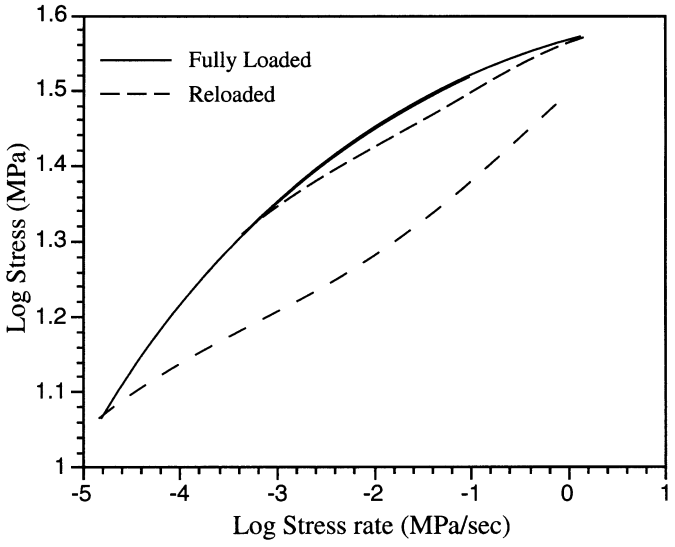

Fig. 14. Plot of log σ versus log $\dot{\sigma}$ for the result of the simulation performed on the relaxation experiment.

It should be noted that σ_t^* does not remain constant during the relaxation. In the event that the unrecoverable plastic strain rate $\dot{\alpha}$ is not negligible the solution is given by including all of the constitutive equations with the requirement that $\dot{\varepsilon} = 0$.

Fig. 12 shows the experimental results for load relaxation experiments performed at different stages of loading (Fig. 13). In reality the relaxation occurred for much longer time and covered a much larger range of strain rates as reflected in Fig. 12. Fig. 13 shows the initial part of the relaxation. The rest shows up as a straight vertical line that would not produce any additional information and was omitted in the figure. The path back to the main cycle is as shown in the figure. The strains before relaxation correspond well to each other for the two figures. Fig. 14 shows the result of the numerical simulation for the load relaxation experiments performed at different stages of loading. The difference can be explained on the values of the transient stress at the beginning of the test. During the loading process σ_t gradually decreases and its transient contribution gradually diminishes. The stress level increases by a very small amount during this process. At full loading no transient is observed since σ_t becomes zero (Fig. 14). This, however, requires a large amount of strain (1%). All the parameters for this experiment are the same as the ones used for the load relaxation experiment.

6. Conclusion

A transient model is presented here based on Hart's original model. The results show that the model not only captures the cyclic behavior but also predicts the transients in load relaxation experiments. The new model introduces a new state variable in the form of a micro-harness parameter. The new state variable is a measure of the small barriers to the mobile dislocation density whereas the hardness parameter originally proposed by Hart represents the strength of the strong barriers to dislocation motion (forest dislocation, grain boundaries, etc.). A steady-state condition is proposed which reduces the model to the conventional Hart's model for inelastic deformation of polycrystalline materials. Most of the model parameters can be determined from the steady state condition and a methodology is introduced to measure the other parameters from a novel experimental technique based on the control of the inelastic strain rate.

References

Alden, T.H., 1977. Load relaxation in aluminum: I. Theory of plastic deformation. II. Plastic equation of state. Metallurgical Transactions A 8A, 1675–1687.

Alden, T.H., 1987. Theory of plastic and viscous deformation. Metallurgical Transactions A 18A, 811–826.

Alexopoulos, P.S., Keusseyan, R.L., Wire, G.L., Li, C.Y., 1982. Mechanical testing for deformation model development. In: Rohde, R.W., Swearengen, J.C. (Eds.) ASTM Publication V. STP 765. pp. 148.

Arnold, S.M., Saleeb, A.F., 1994. On the thermodynamic framework of generalized coupled thermo-elastic-viscoplastic-damage modelling. Int. J. Plasticity 10, 263–278.
Arnold, S.M., Saleeb, A.F., Wilt, T.E., 1995. Modeling investigation of thermal and strain induced recovery and nonlinear hardening in potential based viscoplasticity. Eng. Mater. Technol. 117, 157–167.
Arnold, S.M., Saleeb A.F., Castelli, M.G., 1996. Fully associative, nonisothermal, nonlinear kinematic, unified viscoplastic model for titanium alloys. In: Proc. 2nd Symposium on Thermomechanical Fatigue Behavior of Materials, Phoenix, AZ, pp. 146–173.
Dewhurst, T.B., Dawson, P.R., 1984. Analysis of large plastic deformations at elevated temperatures using state variable models for viscoplastic flow. In: Proc. 1984 Winter Annual Meeting of the ASME. New Orleans, LA, pp. 149–163.
Essmann, U., Mughrabi, H., 1979. Annihilation of dislocations during tensile and cyclic deformation and limits of dislocation densities. Philos. Mag. A 40, 731–756.
Faruque, M.O., Zaman, M., Hossein, M.I., 1996. Creep constitutive modeling of an aluminum alloy under multiaxial and cyclic loading. International Journal of Plasticity 12 (6), 761–780.
Ferron, G., Mliha-Touati, M., 1987. Phenomenological study of the plastic behavior of aluminum at low and medium temperatures. Acta Metall. 35, 1281–1288.
Follansbee, P.S., Kocks, U.F., 1988. Constitutive description of the deformation of copper based on the use of the mechanical threshold stress as an internal state variable. Acta Metall. 36, 81–93.
Gilat, G., Wu, X., 1997. Plastic deformation of 1020 steel over a wide range of strain rates and temperatures. International Journal of Plasticity 13 (6–7), 611–632.
Hannula, S., 1988. State variable approach to deformation phenomena in fcc metals. In Publications of Technical Research Center of Finland, pp. 1–40.
Hart, E.W., 1976. Constitutive relations for nonelastic deformation of metals. J. Eng. Mater. Technol. 98, 193–202.
Hart, E.W., 1984. A micromechanical basis for constitutive equations with internal state variables. Eng. Mater. Technol. 106, 322–325.
Hart, E.W., Garmestani, H., 1993. Mechanical testing using direct control of the inelastic strain rate. Experimental Mechanics 1–6.
Hart, E.W., Solomon, H.D., 1973. Load relaxation studies of polycrystalline high purity aluminium. Acta Metall. 21, 295–307.
Horstemeyer, M.F., McDowell, D.L., 1995. Stress state and history effects in viscoplasticity at finite strain. In: Proc. 1995 ASME International Mechanical Engineering Congress and Exposition. Part 1, San Francisco, CA, pp. 519–543.
Jackson, M.S., Cho, C.W., Alexopoulos, P., Li, C.Y., 1981. Phenomenological model for transient deformation based on state variables. Eng. Mater. Technol. 103, 314–325.
Khan, A.S., Liang, R., 1999. Behavior of three BCC metal over a wide range of strain rates and temperaturs: experiments and modelling. International Journal of Plasticity 15, 1089–1109.
Khraisheh, M.K., Zbib, M.H., Hamilton, C.H., Bayoumi, A.E., 1997. Constitutive modeling of superplastic deformation. Part I: theory and experiments, Vol. 13, No. 1/2, pp. 143-164.
Krausz, A., Krausz, K. (Eds.), 1996. Unified Constitutive Laws of Plastic Deformation. Academic Press, San Diego.
Krieg, R.D., Swearengen, J.C., Rohde, R.W., 1978. Inelastic behavior of pressure vessel and piping components. In: Chang, T.Y., Krempl, E. (Eds.), ASME Publication PVP-PB-028. pp. 15.
Lee, D., Hart, E.W., 1971. Stress relaxation and mechanical behavior of metals. Metallurgical Transactions 2, 1245–1248.
Miller, A.J., 1976a. An inelastic constitutive model for monotonic, cyclic, and creep deformation: Part I — equations development and analytical procedures. Eng. Mater. Technol. 96, 97–105.
Miller, A.J., 1976b. An inelastic constitutive model for monotonic, cyclic, and creep deformation: Part II — application to type 304 stainless steel. Eng. Mater. Technol. 96, 106–112.
Nemat-Nasser, S., 1983. On finite plastic flow of crystalline solids and geomaterials. J. Appl. Mech. 50, 1114–1126.
Nemat-Nasser, S., Chung, D.T., Taylor, L.M., 1989. Phenomenological modeling of rate-dependent plasticity for high strain rate problems. Mech. Mater. 7, 319–344.

Robinson, D.N., 1983. Constitutive relationships for anisotropic high-temperature alloys. Nuclear Engineering and Design 83, 389–396.

Sample, V.M., Jaworski, A.P., Field, D.P., 1993. Comparison of parameter evaluation procedures for a two-internal state variable constitutive model. In: Proc. 1993 Winter Annual Meeting of the ASME, New Orleans, LA, pp. 227–242.

Simo, J.C., Hughes, T.J.R., 1997. Computational Inelasticity. Springer Verlag, New York, Berlin, Heildelberg.

Tanner, A.B., McGinty, R.D., McDowell, D.L., 1999. Modeling temperature and strain rate history effects in OFHCCu. Int. J. Plasticity 15(6), 575–603.

Wang, P.T., Richmond, O., 1992. Overview of a two-state variable constitutive model for the consolidation and forming processes of powder-based porous metals. In: Proc. 1992 Winter Annual Meeting of the ASME, Anaheim, CA, pp. 63–83.

Zener, C.M., 1984. Elasticity and Anelasticity of Metals. University of Chicago Press, Chicago.